ARL-TR-95-25

Copy No. 14

Bistatic Scattering and Depth Dependent Gas Fractions in the Acoustic Modeling of Gassy Sediment

Technical Report under Contract N00039-91-C-0082
TD No. 01A2049, Sensor and Environmental Support for MTEDS

Frank A. Boyle
Nicholas P. Chotiros

Applied Research Laboratories
The University of Texas at Austin
P. O. Box 8029 Austin, TX 78713-8029

7 September 1995

Technical Report

Approved for public release;
distribution is unlimited.

Prepared for:
Naval Research Laboratory
Stennis Space Center, MS 39529-5004

Monitored by:
Space and Naval Warfare Systems Command
Department of the Navy
Arlington, VA 22245-5200

DISCLAIMER NOTICE

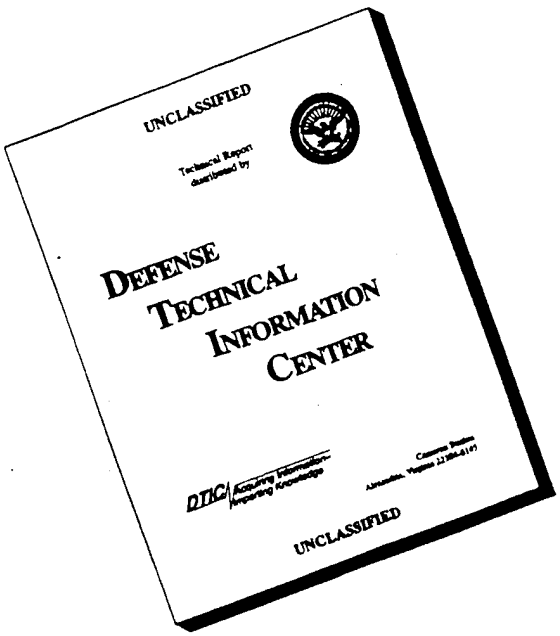

THIS DOCUMENT IS BEST QUALITY AVAILABLE. THE COPY FURNISHED TO DTIC CONTAINED A SIGNIFICANT NUMBER OF PAGES WHICH DO NOT REPRODUCE LEGIBLY.

REPORT DOCUMENTATION PAGE

Form Approved
OMB No. 0704-0188

1. AGENCY USE ONLY (Leave blank)	2. REPORT DATE	3. REPORT TYPE AND DATES COVERED
	7 Sep 95	technical

4. TITLE AND SUBTITLE

Bistatic Scattering and Depth Dependent Gas Fractions in the Acoustic Modeling of Gassy Sediment, Technical Report under Contract N00039-91-C-0082, TD No. 01A2049, Sensor and Environmental Support for MTEDS

5. FUNDING NUMBERS

N00039-91-C-0082,
TD No. 01A2049

6. AUTHOR(S)

Boyle, Frank A. Chotiros, Nicholas P.

7. PERFORMING ORGANIZATION NAMES(S) AND ADDRESS(ES)

Applied Research Laboratories
The University of Texas at Austin
P.O. Box 8029
Austin, Texas 78713-8029

8. PERFORMING ORGANIZATION REPORT NUMBER

ARL-TR-95-25

9. SPONSORING/MONITORING AGENCY NAME(S) AND ADDRESS(ES)

Naval Research Laboratory
Stennis Space Center, MS 39529-5004

Space and Naval Warfare Systems Command
Department of the Navy
Arlington, VA 22245-5200

10. SPONSORING/MONITORING AGENCY REPORT NUMBER

11. SUPPLEMENTARY NOTES

12a. DISTRIBUTION/AVAILABILITY STATEMENT

Approved for public release; distribution is unlimited.

12b. DISTRIBUTION CODE

13. ABSTRACT (Maximum 200 words)

A model for acoustic scattering from the seabed was previously developed by Boyle and Chotiros [ARL-TR-93-15, "Bottom Backscatter from Trapped Bubbles" and ARL-TR-94-21, "Bottom Backscatter from Trapped Bubbles II"]. The model treats acoustic scattering as a sum of three independent processes, including scattering from the sediment interface, volume scattering from sediment grains, and volume scattering from trapped gas bubbles that might exist between grains. Recently the gas bubble component of this model has been modified to allow for bistatic scattering and depth dependent sediment gas fractions. The theories behind these modifications are described, and in each case the character of the resulting model studied.

14. SUBJECT TERMS

(see reverse side)

15. NUMBER OF PAGES

29

16. PRICE CODE

17. SECURITY CLASSIFICATION OF REPORT	18. SECURITY CLASSIFICATION OF THIS PAGE	19. SECURITY CLASSIFICATION OF ABSTRACT	20. LIMITATION OF ABSTRACT
UNCLASSIFIED	UNCLASSIFIED	UNCLASSIFIED	SAR

14. backscatter
backscattering strength
Biot
bistatic scattering
bubbles
depth dependence
gas fraction
Lambert's rule
reciprocity
seabed
sediment
stratified medium
trapped bubbles

TABLE OF CONTENTS

This page intentionally left blank.

LIST OF FIGURES

This page intentionally left blank.

1. INTRODUCTION

Acoustic backscatter from the seafloor has been a topic of considerable interest over the past several decades. The importance of seabed acoustics has recently grown due to current emphasis on mine warfare in the littoral environment. Since there is at present no general agreement on the physics of the scattering process, a lot of models exist, based on several different hypothetical scattering mechanisms. They include models based on scattering at the sediment interface, like those of Patterson[1] and Clay and Medwin,[2] as well as the volume scattering models of Nolle,[3] Stockhausen,[4] and Ivakin and Lysanov.[5] Jackson et al.[6-8] developed a two-component model that treats interface roughness scattering and volume scattering separately. Applying this model to several sites suggests that both components are important, each dominating the total backscatter prediction in half of six cases.

Jackson's model characterizes the seabed with six parameters, two of which describe the interface roughness and three of which describe acoustic propagation through the sediment, modeled as an acoustic fluid. The remaining parameter is an empirically determined quantity which specifies the level of volume scattering within the sediment. No attempt is made to specify the actual volume scattering mechanisms involved.

In 1990, Chotiros[9] began a comprehensive compilation of all available shallow grazing angle backscatter data published in the literature. The results appeared to show some statistically significant trends that suggest specific volume scattering mechanisms, that might be modeled physically. Two hypothetical scattering mechanisms, involving scattering from sediment grains and from trapped bubbles, appear to fit the general trends in the data. At present the data set is expanding and the trends remain.

In 1992 the results of three acoustic penetration experiments at sea and in the laboratory became available. They suggested that sandy sediments might best be modeled structurally via the Biot poroelastic theory, particularly for high frequencies and shallow grazing angles.

In 1993, under Contract N00039-91-C-0082, (entitled "Bottom Backscatter from Trapped Bubbles"), development of a new backscatter model was begun with the intention of taking advantage of the most recent experimental information. It was continued in 1994 under the same contract. The development is described in two technical reports (ARL-TR-93-15[10] and ARL-TR-94-21[11]). The model, called BOGGART, is intended for minehunting applications and is therefore optimized for shallow grazing angle, high frequency behavior. Like Jackson's model, BOGGART includes volume and interface scattering components. It is different in its modeling of the sediment's structure and in the scattering mechanisms.

BOGGART is unique among current scattering models in two important ways. First, the sediment is modeled structurally via the Biot theory. Second, the volume scattering is modeled physically rather than empirically. BOGGART consists of three modular components that predict partial scattering strengths due to sediment grains, gas bubbles, and interface roughness. Hence the name BOGGART, which is the acronym for bottom grain gas and roughness technique.

This report describes refinements that have been incorporated in BOGGART since ARL-TR-49-21. Both of these affect the trapped gas bubble scattering component of the model. They are (1) a modification to allow computation of bistatic scattering strengths, and (2) depth dependent gas fractions. Section 2 is a review of the expression for the backscattering strength of a sediment, due to trapped gas bubbles in resonance. Section 3 describes the calculation of bistatic scattering strengths. Section 4 describes modeling of sediments with depth dependent gas fractions.

2. BACKSCATTERING STRENGTH OF A GASSY SEDIMENT

Figure 2.1 illustrates a method of determining the acoustic pressure returned to an acoustic source in the water from an element of sediment volume dxdydz below the sediment interface. It is based on the principle of acoustic reciprocity, which states that, in a linear medium, the position of an identical source and receiver can be swapped with no change in the ratio of receive to transmit signals. The swapping of positions can be interpreted to represent the backscatter case where a scatterer acts as an acoustic source and the original projector as a receiver.

The acoustic source and scattering elements are both assumed small in comparison with the acoustic wavelength. Both are surrounded with equal virtual spheres of radius much larger than the wavelength. The backscattering of sound from the volume element can be interpreted as follows. First, the virtual sphere surrounding the source oscillates with surface velocity $\mathbf{v_0}$. This induces an acoustic pressure $\mathbf{p_1}$ at the scattering element. The scatterer responds with its own sphere's surface velocity $\mathbf{v_1}$, which induces an acoustic pressure $\mathbf{p_2}$ back at the source in the water column. These pressures and surface velocities can be related by acoustic reciprocity:

$$\frac{p_1}{v_0} = \frac{p_2}{v_1} \quad . \tag{2.1}$$

The surface velocities $\mathbf{v_0}$ and $\mathbf{v_1}$ can be expressed in terms of local acoustic pressures and impedances:

$$v_0 = \frac{p_0}{z_0} \tag{2.2}$$

$$v_1 = \frac{\varepsilon p_1}{z_1} \quad , \tag{2.3}$$

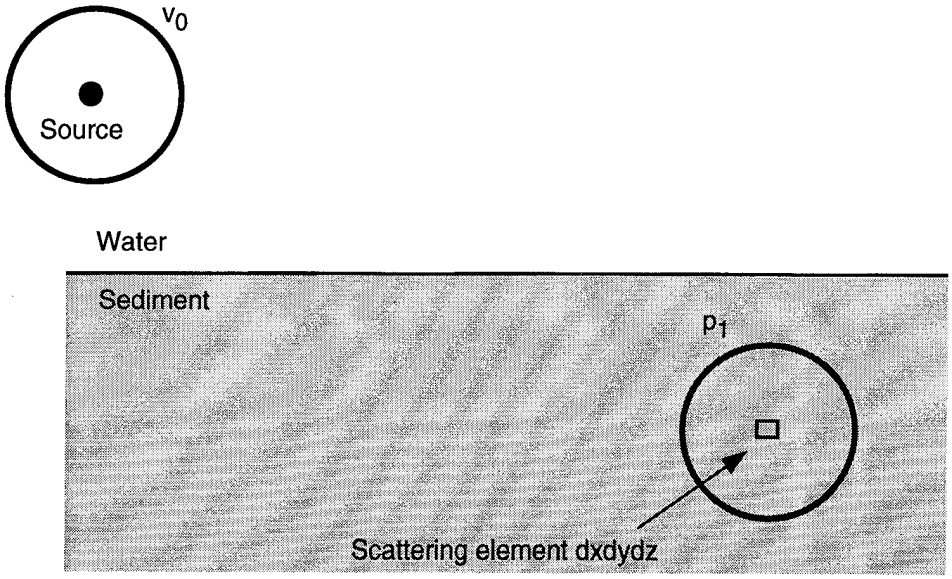

(a) Acoustic propagation of incident sound

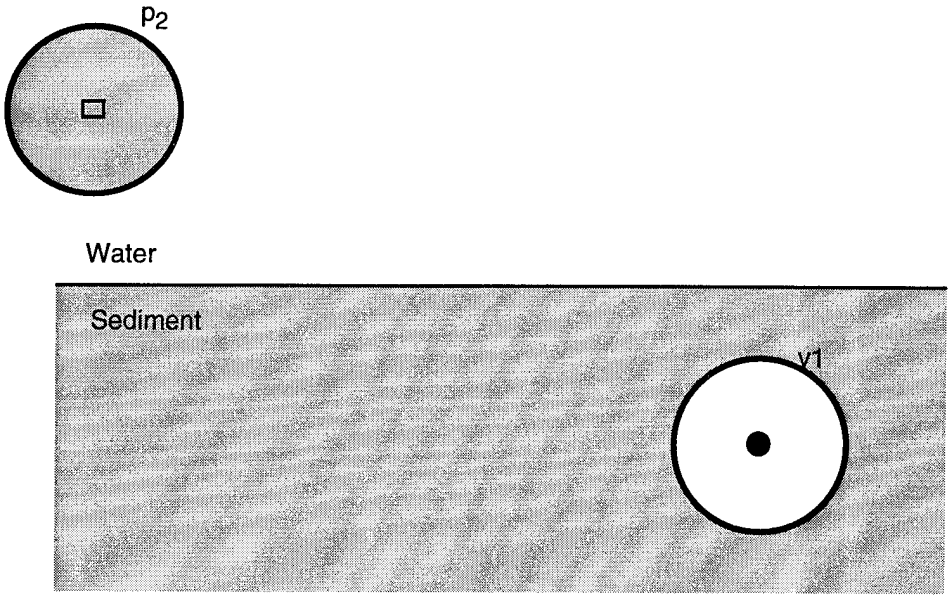

(b) Acoustic propagation of backscattered sound

Figure 2.1
Determining backscattered pressure from an element of sediment volume by acoustic reciprocity.

where $\mathbf{v_0}$, $\mathbf{p_0}$, and $\mathbf{Z_0}$ are the surface velocity, acoustic pressure, and acoustic impedance at the surface of the virtual sphere surrounding the source. $\mathbf{v_1}$, $\mathbf{p_1}$, and $\mathbf{Z_1}$ are the surface velocity, acoustic pressure, and impedance at the sphere surrounding the scatterer. ε is a transfer function from incident pressure upon the scatterer to scattered pressure at its virtual sphere. Its average square magnitude is expressible in terms of the scattering cross section of the volume element:

$$\left\langle |\varepsilon|^2 \right\rangle = \frac{\sigma_{bv} dxdydz}{4\pi r_s^2} \quad , \tag{2.4}$$

where r_s is the chosen radius for the virtual spheres and σ_{bv} is an average scattering cross section per unit volume of sediment. The average is taken over the entire ensemble of possible distributions of scatterers within the volume element. If multiple scattering is neglected, it can be expressed as

$$\sigma_{bv} = \int_0^\infty N(r_b)\sigma(r_b)dr_b \quad , \tag{2.5}$$

where $N(r_b)$ is the bubble size density function and r_b is the bubble radius. The bubble size density function is estimated from the grain size density function, as described in Ref. 10.

Combination of Eqs. (2.1) - (2.4) yields an expression for the pressure returned to the projector from the element dxdydz of sediment volume:

$$\left\langle |\mathbf{p_2}|^2 \right\rangle = \int \left| \frac{\mathbf{p_1}}{\mathbf{p_0}} \right|^2 \frac{\sigma_{bv}}{4\pi r_s^2} \left| \frac{\mathbf{Z_0}}{\mathbf{Z_1}} \mathbf{p_1} \right|^2 dxdydz \quad . \tag{2.6}$$

Recent experiments[12,13] suggest that the best way to model the acoustics of sandy sediments is via the Biot theory for fluid filled porous media.[14-16] Biot's theory predicts two compressional waves to exist in the pore fluid surrounding the bubbles. These waves both contribute to the total backscattered pressure:

$$\left\langle \left| p_2 \right|^2 \right\rangle = \int \left| \frac{p_1}{p_0} \right|^2 \left(\frac{\sigma_{bvf}}{4\pi r_s^2} \left| \frac{Z_0}{Z_{1f}} p_{1f} \right|^2 + \frac{\sigma_{bvs}}{4\pi r_s^2} \left| \frac{Z_0}{Z_{1s}} p_{1s} \right|^2 \right) dxdydz \quad , \qquad (2.7)$$

where Z_{1f}, p_{1f}, Z_{1s}, and p_{1s} are partial acoustic impedances and refracted pressures, obtainable via the Biot theory. σ_{bvf} and σ_{bvs} are scattering cross sections that depend on whether a Biot fast wave or slow wave is being scattered. These quantities are described in more detail in Ref. 11.

The effective scattering p_{bs} from a sediment interface can be regarded as a sum of contributions from all volume elements below the interface. In integral form,

$$\left\langle \left| p_{bs} \right|^2 \right\rangle = \int_0^\infty \left| \frac{p_1}{p_0} \right|^2 \left(\frac{\sigma_{bvf}}{4\pi r_s^2} \left| \frac{Z_0}{Z_{1f}} p_{1f} \right|^2 + \frac{\sigma_{bvs}}{4\pi r_s^2} \left| \frac{Z_0}{Z_1} p_{1s} \right|^2 \right) dz \quad . \qquad (2.8)$$

The backscattering strength of the interface is defined as

$$BS = 10 \log \frac{\left\langle \left| p_s \right|^2 \right\rangle}{\left| p_{inc} \right|^2} \quad , \qquad (2.9)$$

where p_{inc} is the acoustic pressure of a plane wave incident upon a unit area of the sediment interface, and p_s is the pressure of a scattered wave at a distance of 1 m from the interface element, neglecting absorption and scattering within the water column. The pressures p_{inc} and p_s can be related to pressures experienced at the projector, by accounting for spherical spreading and attenuation in the water column,

$$\left| p_s \right| = \left| p_{bs} \right| \frac{r_s}{r_{1m}} e^{r_s \alpha} \quad , \qquad (2.10)$$

$$\left| p_{inc} \right| = \left| p_0 \right| \frac{r}{r_s} e^{-r_s \alpha} \quad , \qquad (2.11)$$

where α is the acoustic absorption in the water column, r_{1m} is the unit radius and r is the distance from the interface element to the projector. Substitution of Eqs. (2.8), (2.10), and (2.11) into Eq. (2.9) yields an expression for the backscattering strength:

$$BS = 10 \log \left(\frac{\left(\frac{1}{r_{1m}^2}\right) \int_0^\infty |p_1|^2 \left(\frac{\sigma_{bvf}}{4\pi} \left| \frac{Z_0}{Z_{1f}} p_{1f} \right|^2 + \frac{\sigma_{bvs}}{4\pi} \left| \frac{Z_0}{Z_{1s}} p_{1s} \right|^2 \right)}{|p_{inc}|^4} \right) \cdot \quad (2.12)$$

This page intentionally left blank.

3. BISTATIC SCATTERING

Figure 3.1 is an illustration of the bistatic scattering problem. A projector at A insonifies an element dxdydz of sediment volume, which scatters sound. A receiver exists in the water column at C. The principle of acoustic reciprocity is invoked to determine a relationship between the sound scattered at B and that measured at C.

The procedure is as follows. First, the scatterer at B and the receiver at C are surrounded by virtual spheres with radius $r_s >> \lambda$. The pressure at B that would be induced by a unit velocity at the surface of the virtual sphere at C can be computed by way of the Biot theory. By reciprocity, the pressure at C due to a unit velocity at the surface of B is the same. This pressure is then multiplied by the scattered surface velocity at B that is produced when B is insonified by the source at A. The square magnitude of pressure at the receiver due to bistatic scattering from a volume element dxdydz is given by

$$\left\langle \left| p_2 \right|^2 \right\rangle = \int_0^\infty \left| \frac{p_b}{p_c} \right|^2 \left(\frac{\sigma_{bvf}}{4\pi r_s^2} \left| \frac{z_0}{Z_{1f}} p_{1f} \right|^2 + \frac{\sigma_{bvs}}{4\pi r_s^2} \left| \frac{z_0}{Z_{1s}} p_{1s} \right|^2 \right) dx dy dz \quad , \qquad (3.1)$$

where p_b is the total pore pressure at the scattering element that would be induced by a pressure p_c at the surface of the virtual sphere of radius r_s surrounding the receiver at C. Just as is done in Eq. (2.8) for the backscatter case, the square pressure from an interface element dxdy is defined as the sum of contributions from all volume elements below dxdy,

$$\left\langle \left| p_{fs} \right|^2 \right\rangle = \int_0^\infty \left| \frac{p_b}{p_c} \right|^2 \left(\frac{\sigma_{bvf}}{4\pi r_s^2} \left| \frac{z_0}{Z_{1f}} p_{1f} \right|^2 + \frac{\sigma_{bvs}}{4\pi r_s^2} \left| \frac{Z_0}{Z_{1s}} p_{1s} \right|^2 \right) dz \quad . \qquad (3.2)$$

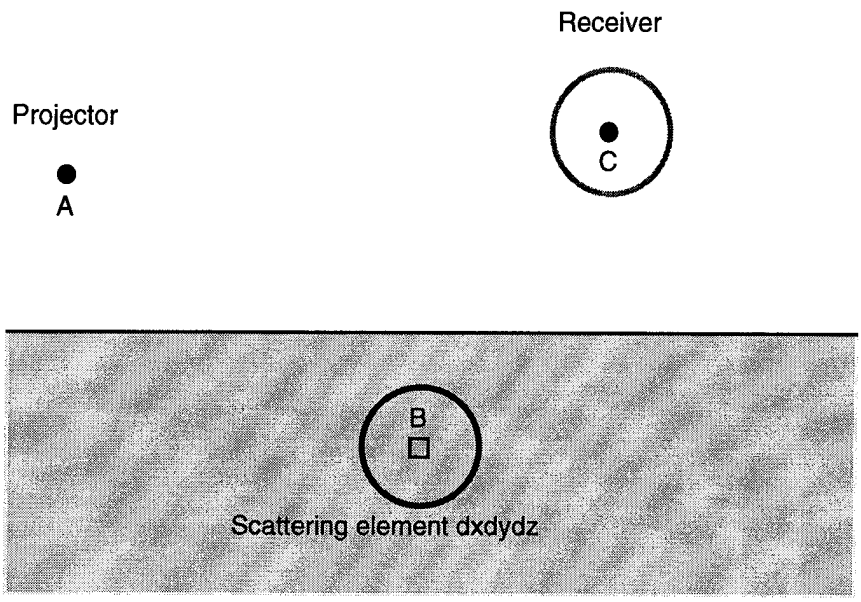

Figure 3.1
Calculation of bistatic scattering strength by reciprocity.

The interface bistatic scattering strength can be defined in terms of the scattered and incident pressures at the interface:

$$SS = 10 \log \frac{\langle p_s^2 \rangle}{|p_{inc}|^2} \quad , \tag{3.3}$$

where p_{inc} is the incident acoustic pressure upon the interface and p_s is the scattered pressure at unit distance from the interface element dxdy. p_s can then be related to the pressure p_{fs} experienced at C by accounting for absorption and spherical spreading:

$$|p_s| = |p_{fs}| \frac{r_c}{r_{1m}} e^{r_c \alpha} \quad , \tag{3.4}$$

where r_c is the distance from surface element dxdy to the receiver. The bistatic scattering strength of the interface is given by substitution of Eqs. (3.2) and (3.4) into Eq. (3.3):

$$SS = 10 \log \left(\frac{\left(\frac{r_c}{r_{1m}}\right)^2 e^{2r_c\alpha} \int_0^\infty \left|\frac{p_b}{p_c}\right|^2 \left(\frac{\sigma_{bvf}}{4\pi r_s^2} \left| \frac{z_0}{Z_{1f}} p_{1f} \right|^2 + \frac{\sigma_{bvs}}{4\pi r_s^2} \left| \frac{Z_0}{Z_{1s}} p_{1s} \right|^2 \right) dz}{|P_{inc}|^2} \right) . \tag{3.5}$$

Figure 3.2 is a plot of the bistatic scattering strength versus incident and exit grazing angle. The modeled sediment is described in Table 3.1. Reflection from the water-sediment interface is not included in this plot. There is no azimuthal dependence since the bubbles are small in comparison with the acoustic wavelength and are excited as monopoles.

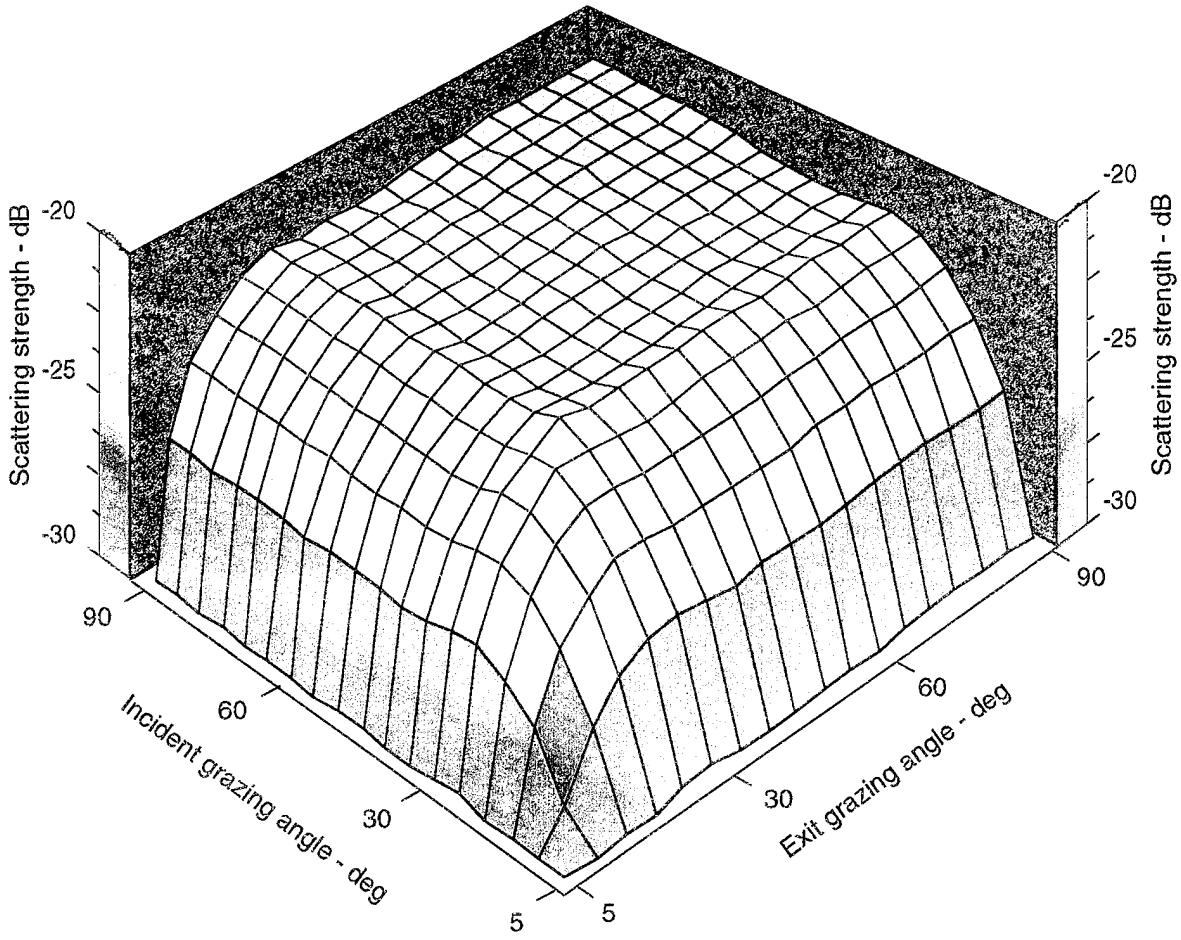

Figure 3.2
Bistatic scattering strength for sediment described in Table 3.1.

Table 3.1
Bistatic scattering model site parameters*.

Fluid Density	(kg/m^3)	1000
Fluid Bulk Modulus	(Pa)	2.25×109
Porosity		0.39
Grain Density	(kg/m^3)	2650
Mean Grain Diameter	(f)	2.51
Standard Deviation	(f)	0.79
Pore Size Parameter	(m)	5.08×10^{-5}
Viscosity	(kg/m-s)	1.0×10^{-3}
Permeability	(m^2)	5.03×10^{-11}
Virtual Mass Parameter		1.782
Grain Bulk Modulus	(Pa)	7.0×109
Frame Shear Modulus	(Pa)	2.61×107
Shear Log Decrement		0.15
Frame Bulk Modulus	(Pa)	5.3×109
Bulk Log Decrement		0.15
Gas Bulk Modulus	(Pa)	2.48×105
Gas Density	(kg/m^3)	1.22
Gas Heat Conductivity	(cal/m-s-°C)	5.6×10^{-3}
Gas Specific Heat (const press)	(cal/kg)	240
Gas Specific Heat Ratio, Cp/Cv		1.4
Bubble Surface Tension	(N/m^2)	0.075
Bubble/Pore Radius Ratio		8.43
Gas Content		1.0×10^{-5}

* Parameters apply to a sandy site near Panama City, Florida[20]

This page intentionally left blank.

4. DEPTH DEPENDENT GAS FRACTIONS

Gassy marine sediments have been observed to be strongly horizontally stratified. In a recent experiment accomplished in the Baltic Sea as part of the Coastal Benthic Boundary Layer Special Research Project,[17] normal incidence echo soundings revealed a bright reflective layer 1 m below the sediment interface. It has been widely speculated that this layer is indicative of trapped gas. The horizontal stratification of this feature suggests that gas content in actual sediments may be strongly depth dependent. Depth dependent gas fractions have been indicated elsewhere, including a laboratory sediment tank at ARL:UT, where an absence of gas in the first few centimeters of sediment has been observed. Hence the motivation for a revised version of Eq. (2.12) that allows for depth dependent gas fractions.

Two of the components of Eq. (2.12) that will be affected by a varying gas fraction are the volume scattering cross sections σ_{bvf} and σ_{bvs}. Each is proportional to the density of scatterers and therefore to the gas fraction. In the absence of multiple scattering, they are expressed as integrals over all possible bubble radii:

$$\sigma_{bvf} = \int_0^\infty N(r_b)\, \sigma_f(r_b) dr_b \quad , \tag{4.1}$$

$$\sigma_{bvs} = \int_0^\infty N(r_b)\, \sigma_s(r_b) dr_b \quad , \tag{4.2}$$

where r_b is the bubble radius and $N(r_b)$ is the density function of bubble sizes, which is defined as the number of bubbles per unit volume per unit radius increment. σ_f and σ_s are single bubble scattering cross sections for fast and slow waves, respectively. They are given by Wildt:[18]

$$\sigma_f(r_b) = \frac{4\pi r_b^2}{\left[\left(\frac{f_{rf}}{f}\right)^2 - 1\right]^2 + \delta_f^2} \quad , \tag{4.3}$$

$$\sigma_f(r_b) = \frac{4\pi r_b^2}{\left[\left(\frac{f_{rf}}{f}\right)^2 - 1\right]^2 + \delta_f^2} \quad , \tag{4.4}$$

where f is the acoustic frequency, f_{rf} and f_{rs} are resonance frequencies involving fast and slow waves, and δ_f and δ_s are damping constants for fast and slow waves. Detailed expressions for each of these parameters are given in Ref. 2.

The bubble size density function $N(r_b)$ can be expressed as a product of the gas fraction ζ and a normalized bubble size density function $F(r_b)$:

$$N(r_b) = \zeta F(r_b) \quad . \tag{4.5}$$

Upon substitution of Eqs. (4.5), (4.1), and (4.2) into Eq. (2.12),

$$BS = 10 \log \left(\frac{\int_0^\infty \left(\frac{\sigma_1}{4\pi} \left| \frac{z_0}{Z_{1f}} p_{1f} \right|^2 + \frac{\sigma_2}{4\pi} \left| \frac{z_0}{Z_{1s}} p_{1s} \right|^2 \right) \left| P_{bf} + P_{bs} \right|^2 dz}{\left| P_{inc} \right|^4} \right) \quad , \tag{4.6}$$

where σ_1 and σ_2 are defined by

$$\sigma_1 = \int_0^\infty F(r_b)\sigma_f(r_b)\, dr_b \quad , \tag{4.7}$$

$$\sigma_2 = \int_0^\infty F(r_b)\sigma_s(r_b)\, dr_b \quad . \tag{4.8}$$

Other factors in Eq. (4.6) that can be affected by a depth dependent gas fraction are the refracted acoustic pressures p_{bf} and p_{bs} carried by the Biot fast and slow waves. These pressures can be expected to vary in the presence of

trapped gas, which scatters and absorbs sound. The fast and slow wave pressures $p_{bf}(z)$ and $p_{bs}(z)$ in a gassy sediment can be expressed as

$$p_{bf}(Z) = p_{bf0}(Z)\,\beta_f(Z) \quad , \tag{4.9}$$

$$p_{bs}(Z) = p_{bs0}(Z)\,\beta_s(Z) \quad , \tag{4.10}$$

where $p_{bf0}(z)$ and $p_{bs0}(z)$ are the fast and slow wave acoustic pressures that would exist if no gas were present. $\beta_f(z)$ and $\beta_s(z)$ are multipliers that adjust for scattering and absorption of sound by trapped gas. They can be expressed in terms of the sediment's depth dependent extinction cross section,

$$\beta_f(z) = \exp\left[-\int_0^z \frac{\sigma_{fev}(Z_1)}{\sin\Phi}\,dz_1\right] \quad , \tag{4.11}$$

$$\beta_s(z) = \exp\left[-\int_0^z \frac{\sigma_{sev}(Z_1)}{\sin\Phi}\,dz_1\right] \quad , \tag{4.12}$$

where Φ is the grazing angle. The fast and slow wave sediment extinction cross sections $\sigma_{fev}(z)$ and $\sigma_{sev}(z)$ can be expressed in terms of the gas fraction and the bubble size density function,

$$\sigma_{fev}(Z_1) = \zeta(Z_1)\int_0^\infty F(r_b)\,\sigma_{fe}(r_b)\,dr_b \quad , \tag{4.13}$$

$$\sigma_{sev}(Z_1) = \zeta(Z_1)\int_0^\infty F(r_b)\,\sigma_{se}(r_b)\,dr_b \quad , \tag{4.14}$$

where $\zeta(z_1)$ is the depth dependent gas fraction and $F(r_b)$ is the bubble size density function. $\sigma_{fe}(r_b)$ and $\sigma_{se}(r_b)$ are the fast and slow wave extinction cross sections of a single bubble of radius r_b, given by Wildt.[18]

$$\sigma_{fe}(r_b) = \sigma_f(r_b)\,\frac{\delta_f}{kr_b} \quad , \tag{4.15}$$

$$\sigma_{se}(r_b) = \sigma_s(r_b)\frac{\delta_s}{kr_b} \quad , \tag{4.16}$$

where $\sigma_f(r_b)$ and $\sigma_s(r_b)$ are the fast and slow wave scattering cross sections, δ_f and δ_s are the corresponding damping constants, and k is the acoustic wavenumber.

Figure 4.1 illustrates the effect of depth dependent gas fractions on the backscattering strength. It is a comparison of predicted backscattering strength versus grazing angle over a sandy sediment bottom with different gas fraction profiles. The sediment geoacoustic parameters are those listed in Table 4.1. The gas fraction profiles include (1) an infinite homogeneous half space with gas fraction of 10^{-5}, (2) a 7 cm gasless layer over an infinite half space with gas fraction of 10^{-5}, and (3) a 20 cm gasless layer over an infinite half space with gas fraction of 10^{-5}.

In Fig. 4.1, the predicted backscattering strengths have been shifted vertically to line up the initial portions of the scattering strength curves. It is apparent from this figure that in addition to decreasing the backscattering strength, the addition of a gasless layer has the effect of causing the backscattering strength to increase more sharply with grazing angle. The dashed curve in Fig. 4.1 is a plot of Lambert's rule, defined as

$$BS = 20\log(\sin\theta) + \eta \quad , \tag{4.17}$$

where θ is the grazing angle and η is a constant, which can be determined by a fit to experimental data. Lambert's rule has been widely observed to fit closely to experimental data,[20] but has no rigorous theoretical grounding. In Fig. 4.1, Lambert's rule appears to follow the 7 cm layer data most closely. This suggests that, in the case of scattering by sediment bubbles, Lambert's rule scattering may be a manifestation of depth dependent scattering properties.

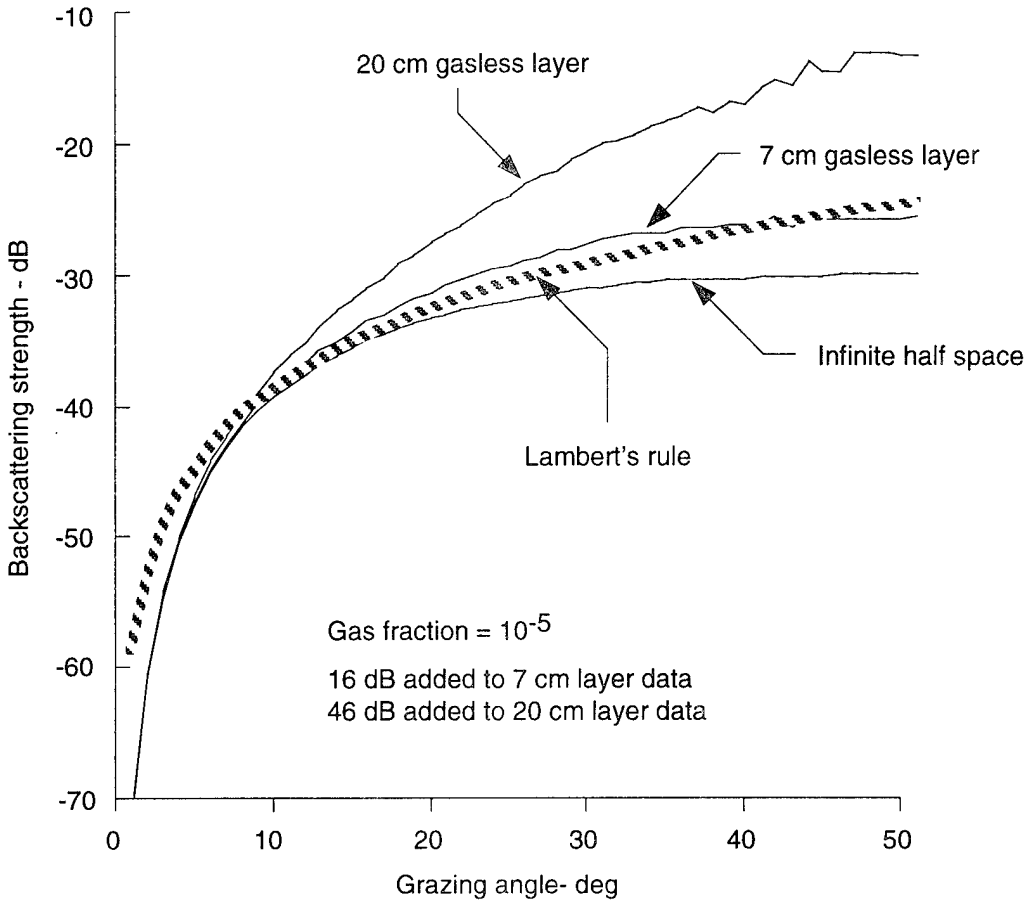

Figure 4.1
Backscattering strength versus grazing angle for different gas fraction profiles. Sediment parameters are given in Table 4.1.

ARL - UT
AS-95-1089
HCB/RFO
12-95/svr

Table 4.1
Site parameters for sediment of Fig. 4.1.

Fluid Density	(kg/m^3)	1000
Fluid Bulk Modulus	(Pa)	2.25×10^{9}
Porosity		0.5
Grain Density	(kg/m^3)	2650
Mean Grain Diameter	(ϕ)	3.0
Standard Deviation	(ϕ)	1.0
Pore Size Parameter	(m)	6.74×10^{-5}
Viscosity	(kg/m-s)	1.0×10^{-3}
Permeability	(m^2)	1.13×10^{-10}
Virtual Mass Parameter		1.5
Grain Bulk Modulus	(Pa)	7.0×10^{9}
Frame Shear Modulus	(Pa)	2.61×10^{7}
Shear Log Decrement		0.15
Frame Bulk Modulus	(Pa)	5.3×10^{9}
Bulk Log Decrement		0.15
Gas Bulk Modulus	(Pa)	2.48×10^{5}
Gas Density	(kg/m^3)	1.22
Gas Heat Conductivity	(cal/m-s-^oC)	5.6×10^{-3}
Gas Specific Heat (const press)	(cal/kg)	240
Gas Specific Heat Ratio, C_p/C_v		1.4
Bubble Surface Tension	(N/m^2)	0.075
Bubble/Pore Radius Ratio		3.42
Gas Fraction Below Layer		1.0×10^{-5}

5. CONCLUSIONS

The ARL:UT bottom backscatter model, BOGGART, has been improved in two ways. Both of these improvements affect the trapped bubble scattering component of the model.

The model has been generalized for bistatic scattering from trapped gas bubbles. The technique is derived from the principle of acoustic reciprocity, which depends on an assumption that scatterers are small in comparison with the acoustic wavelength. The resulting bistatic model has no azimuthal dependence. It is possible that a more complete bistatic scattering model, including sediment grain and roughness components, will have some azimuthal dependence.

Depth dependent gas fractions have been incorporated in the model. Comparisons of different gas fraction profiles suggest that the grazing angle dependence of the backscattering strength is strongly affected. At present the gas fraction is the only parameter in the model that is allowed to vary with depth. A more complete model would allow for depth dependence of other important components, such as the bubble size density function and the Biot parameters.

The current improvements will give BOGGART greater applicability to actual sediments, in which horizontal layering is probably common. The modification for bistatic scattering will help a user make sonar performance predictions in a multipath environment. Though BOGGART is complete and functional, it is modular and designed with future upgrades in mind. Improvements will continue as more experimental information about the seafloor becomes available.

This page intentionally left blank.

REFERENCES

1. R. E. Patterson, "Backscatter of Sound from a Rough Boundary," J. Acoust. Soc. Am. 35, 2010-2013 (1963).

2. C. S. Clay and H. Medwin, *Acoustical Oceanography: Principles and Applications* (Wiley-Interscience, New York, 1977).

3. A. W. Nolle, W. A. Hoyer, J. F. Mifsud, W. R. Runyan, and M. B. Ward, "Acoustic Properties of Water-Filled Sands," J. Acoust. Soc. Am. 35, 1394 (1963).

4. J. H. Stockhausen, "Scattering from the Volume of an Inhomogeneous Half-Space," NRE Report No. 63/9, Naval Research Establishment, Nova Scotia (1963).

5. A. N. Ivakin and Yu. P. Lysanov, "Underwater Sound Scattering by Volume Inhomogeneities of a Bottom Medium Bounded by a Rough Surface," Sov. Phys. Acoust. 27, 212-215 (1981).

6. D. R. Jackson, D. P. Winebrenner, and A. Ishimaru, "Application of the Composite Roughness Model to High-Frequency Bottom Backscattering," J. Acoust. Soc. Am. 79, 1410-1422 (1986).

7. P. D. Mourad and D. R. Jackson, "High-Frequency Sonar Equation Models for Bottom Backscatter and Forward Loss," in Proceedings of Oceans '89 (Marine Technology Society and IEEE, 1989), 1168-1175.

8. D. R. Jackson and K. B. Briggs, "High-Frequency Bottom Backscattering: Roughness versus Interface Scattering," J. Acoust. Soc. Am. 92, 962-977 (1992).

9. N. P. Chotiros and F. A. Boyle, "Gas Bubbles in Ocean Sediments and High-Frequency Acoustic Backscattering Strength," presented at 121st Meeting of the Acoustical Society of America; J. Acoust. Soc. Am. 89(4), Pt. 2, 1852 (1991).

10. F. A. Boyle and N. P. Chotiros, "Bottom Backscatter from Trapped Bubbles," Applied Research Laboratories Technical Report No. 93-15 (ARL-TR-93-15), Applied Research Laboratories, The University of Texas at Austin, July 1993.

11. F. A. Boyle and N. P. Chotiros, "Bottom Backscatter from Trapped Bubbles - II," Applied Research Laboratories Technical Report No. 94-21 (ARL-TR-94-21), Applied Research Laboratories, The University of Texas at Austin, December 1994.

12. N. P. Chotiros and M. L. Ramaker, "High Frequency Acoustic Penetration of Sandy Ocean Sediments," presented at 121st Meeting of the Acoustical Society of America; J. Acoust. Soc. Am. 89(4), Pt. 2, 1908 (1991).

13. F. A. Boyle and N. P. Chotiros, "Experimental Detection of a Slow Acoustic Wave in Sediment at Shallow Grazing Angles," J. Acoust. Soc. Am. 91, 2615-2619 (1992).

14. M. A. Biot, "Theory of Propagation of Elastic Waves in a Fluid Saturated Porous Solid, I. Low Frequency Range," J. Acoust. Soc. Am. 28, 168-178 (1956).

15. M. A. Biot, "Theory of Propagation of Elastic Waves in a Fluid Saturated Porous Solid, II. Higher Frequency Range," J. Acoust. Soc. Am 28, 179-191 (1956).

16. M. Stern, A. Bedford, and H. R. Millwater, "Wave Reflection from a Sediment Layer with Depth-Dependent Properties," J. Acoust. Soc. Am. 77, 1781-1788 (1985).

17. Personal Communication, D. Walter, Naval Research Laboratory, Stennis Space Center, Bay St. Louis, Mississippi.

18. R. Wildt, ed., "Acoustic Theory of Bubbles," in *Physics of Sound in the Sea*, N.D.R.C. Summary Technical Report Div. 6, (Washington, D.C., 1946),Vol. 8, Chap. 28.

19. N. P. Chotiros, "Biot Model of Sound Propagation in Water-Saturated Sand," J. Acoust. Soc. Am. 97(1), 199-214 (1995).

20. R. J. Urick, *Principles of Underwater Sound*, 3rd Edition (McGraw-Hill Book Co., Inc., New York, 1983).

7 September 1995

DISTRIBUTION LIST
ARL-TR-95-25
Technical Report under Contract N00039-91-C-0082,
TD No. 01A2049, Sensor and Environmental Support for MTEDS

Copy No.	
	Commanding Officer Naval Research Laboratory Stennis Space Center, MS 39529-5004
1-3	Attn: S. Tooma (Code 7430)
4	D. Lott (Code 7431)
5	E. Franchi (Code 7100)
6	S. Stanic (Code 7174)
7	D. Ramsdale (Code 7170)
8	M. Richardson (Code 7431)
9	R. Meredith (Code 7174)
10	Library (Code 7032.2)
	Office of Naval Research San Diego Regional Office 4520 Executive Drive, Suite 300 San Diego, CA 92121-3019
11	Attn: J. Starcher, ACO
	Director Naval Research Laboratory Washington, DC 20375
12	Attn: Code 2627
13	B. Houston (Code 5136)
	DTIC-OCC Defense Technical Information Center 8725 John J. Kingman Road, Suite 0944 Fort Belvoir, VA 22060-6218
14 - 25	Attn: Library
	Director Research Program Department Office of Naval Research Ballston Tower One Arlington, VA 22217-5000
26	Attn: J. Simmen (Code 321)
27	E. Chaika (Code 322)
28	W. Ching (Code 321)
29	T. Goldsberry (Code 322)
30	D. Houser (Code 333)

Copy No.

Commander
Naval Meteorology & Oceanography Command
Stennis Space Center, MS 39522-5000
31 Attn: D. Durham (N5A)
32 R. Martin (N5C)

Commander
Program Executive Office - Mine Warfare
Crystal Plaza Bldg. 6
2531 Jefferson Davis Highway
Arlington, VA 22242-5167
33 Attn: J. Grembi (PEOMIW)
34 D. Gaarde (PMO407B)

G & C Systems Manager
MK48/ADCAP Program Office
National Center 2
2521 Jefferson Davis Hwy., 12W32
Arlington, VA 22202
35 Attn: H. Grunin (PMO402E1)

Program Manager
MK50 Torpedo Program Office
Crystal Park 1
2011 Crystal Drive, Suite 1102
Arlington, VA 22202
36 Attn: A. Knobler (PMO406B)

Commander
Dahlgren Division
Naval Surface Warfare Center
Dahlgren, VA 22448-5000
37 Attn: Library

Commander
Dahlgren Division
Naval Surface Warfare Center
Silver Spring, MD 20903-5000
38 Attn: S. Martin (G94)
39 J. Sherman (N50)
40 M. Stripling (N04W)

Distribution List for ARL-TR-95-25 under Contract N00039-91-C-0082, TD No. 01A2049 (cont'd)

Copy No.

Director
Applied Physics Laboratory
The University of Washington
1013 NE 40th Street
Seattle, WA 98105

41 Attn: R. Spindel
42 D. Jackson
43 K. Williams
44 S. Kargl

Director
Life Sciences Directorate
Office of Naval Research
Arlington, VA 22217-5000

45 Attn: S. Zornetzer (Code 114)

Director
Marine Physical Laboratory
The University of California, San Diego
San Diego, CA 92152

46 Attn: K. Watson
47 C. de Moustier

Commander
Mine Warfare Command
325 Fifth St., SE
Corpus Christi, TX 78419-5032

48 Attn: G. Pollitt (N02R)

Applied Research Laboratory
The Pennsylvania State University
P.O. Box 30
State College, PA 16804-0030

49 Attn: L. Hettche
50 R. Goodman
51 E. Liszka
52 Library
53 D. McCammon
54 F. Symons

Copy No.

	National Center for Physical Acoustics University of Mississippi Coliseum Drive University, MS 38677
55	Attn: J. Sabatier
	Commanding Officer Coastal Systems Station, Dahlgren Division Naval Surface Warfare Center Panama City, FL 32407-5000
56	Attn: M. Hauser (Code 10CD)
57	R. Lim (Code 130B)
58	E. Linsenmeyer (Code 10P)
59	D. Todoroff (Code 130)
	Commander Naval Undersea Warfare Center Division New London, CT 06320-5594
60	Attn: J. Chester (Code 3112)
61	P. Koenig (Code 33A)
	Advanced Research Projects Agency 3701 North Fairfax Drive Arlington, VA 22203-1714
62	Attn: W. Carey
	Commander Naval Undersea Warfare Center Division Newport, RI 02841-5047
63	Attn: J. Kelly (Code 821)
64	F. Aidala (Code 842)
65	W. Gozdz (Code 843)
	Physics Department The University of Texas at Austin Austin, TX 78712
66	Attn: T. Griffy
	Aerospace Engineering Department The University of Texas at Austin Austin, TX 78712
67	Attn: M. Bedford
68	M. Stern

Distribution List for ARL-TR-95-25 under Contract N00039-91-C-0082, TD No. 01A2049 (cont'd)

Copy No.	
69	Robert A. Altenburg, ARL:UT
70	Hollis Boehme, ARL:UT
71	Frank A. Boyle, ARL:UT
72	Nicholas P. Chotiros, ARL:UT
73	John M. Huckabay, ARL:UT
74	Thomas G. Muir, ARL:UT
75	Library, ARL:UT
76 - 82	Reserve, ARL:UT